



Fabrication and characterization of $\text{TiO}_2/\text{ZrO}_2$ ceramic membranes for nanofiltration

Honglin Guo ^a, Shuaifei Zhao ^{a, b, *}, Xiaoxian Wu ^a, Hong Qi ^{a, **}

^a State Key Laboratory of Material-Oriented Chemical Engineering, Membrane Science and Technology Research Center, Nanjing Tech University, Nanjing 210009, Jiangsu, China

^b Faculty of Science & Engineering, Macquarie University, NSW 2109, Australia



ARTICLE INFO

Article history:

Received 15 January 2016

Received in revised form

19 February 2016

Accepted 9 March 2016

Available online 10 March 2016

Keywords:

Ceramic membrane

Nanofiltration

Sol–gel

Membrane characterization

Inorganic membrane

ABSTRACT

$\text{TiO}_2/\text{ZrO}_2$ ceramic nanofiltration membranes are successfully fabricated through the polymeric sol–gel route followed by the dip-coating technique. Disk type α -alumina supported mesoporous γ -alumina (pore size: 5–6 nm) is employed as the support in dip-coating. The unsupported and supported composite ceramic membranes are systematically characterized and evaluated in terms of phase composition, chemical stability, gas adsorption, molecular weight cut-off (MWCO), membrane pore size, water flux and salt rejection. It is found that the $\text{TiO}_2/\text{ZrO}_2$ ceramic membranes have amorphous phase at 400 and 500 °C, suggesting the high thermal stability. The fabricated membranes have the MWCO of 620–860 Da, corresponding to the membrane pore size of 1.2–1.5 nm. Relatively low water permeability can be attributed to the low microporosity of the membrane. Donnan exclusion is the dominant transport mechanism of the NF membrane in the single-component system, and salt rejection is closely related to the hydration properties of the ions (e.g., the hydration radius).

© 2017 Elsevier Inc. All rights reserved.

1. Introduction

Nanofiltration (NF), as a pressure driven membrane process with separation properties between ultrafiltration and reverse osmosis, has attracted growing interest in many applications, such as desalination, wastewater treatment and drinking water purification [1–4]. NF membranes are generally divided into two categories according to the material difference, including organic (polymeric) and inorganic ones. Commercial organic (i.e., polymeric) NF membranes have found various industrial applications. However, these organic membranes suffer from some disadvantages, such as low thermal and chemical stabilities and poor mechanical strength. These drawbacks can be overcome by developing more efficient ceramic NF membranes [5,6]. Polymeric nanofiltration membranes are generally used to treat liquids with temperatures below 70 °C, while inorganic nanofiltration membranes

have larger working temperature range, typically can be up to 120 °C (liquids will be vaporized if the temperature is over 120 °C).

Currently, different types of oxide materials have been employed in the development of ceramic NF membranes. These oxide materials include $\gamma\text{-Al}_2\text{O}_3$ [6–9], TiO_2 [10–14], ZrO_2 [15–17], HfO_2 [18,19]. Among them, $\gamma\text{-Al}_2\text{O}_3$ NF membranes have insufficient chemical stability under harsh conditions, which limits their industrial applications [17]. TiO_2 and ZrO_2 materials have relatively high chemical stabilities, making them gain much popularity in the development of ceramic NF membranes [10–17]. However, pure TiO_2 and ZrO_2 ceramic NF membranes may encounter some issues like low thermal stability due to low phase transition temperature, film cracking, large membrane pore size and low selectivity [20–22].

To achieve better performance, composite ceramic NF membranes have been proposed and investigated. Tsuru et al. prepared $\text{SiO}_2/\text{ZrO}_2$ composite NF membranes to improve the stability of SiO_2 membrane in aqueous solutions [23,24]. Recently, Cai et al. fabricated $\text{Pb}\text{-TiO}_2$ membranes via the colloidal sol–gel process and achieved much higher salt rejections compared with the undoped TiO_2 membranes [25]. $\text{TiO}_2/\text{ZrO}_2$ ceramic membranes were also fabricated, and the prepared composite membranes exhibited improved thermal stabilities due to the increase in crystallisation

* Corresponding author. Faculty of Science & Engineering, Macquarie University, NSW 2109, Australia.

** Corresponding author.

E-mail addresses: zhasy001@mymail.unisa.edu.au (S. Zhao), hqi@njtech.edu.cn (H. Qi).

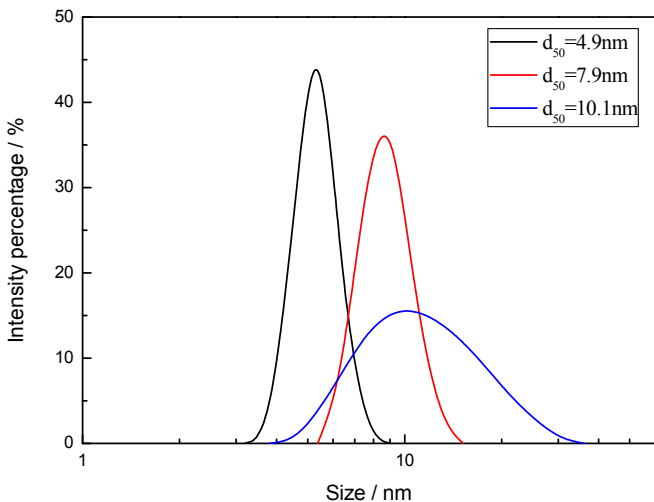


Fig. 1. Particle size distributions of the $\text{TiO}_2/\text{ZrO}_2$ composite sols.

temperature and smaller pore sizes because of the mutual impediment of TiO_2 and ZrO_2 during crystallisation and growing processes [22]. Zeidler et al. successfully developed $\text{TiO}_2/\text{ZrO}_2$ membranes with integrated carbon and improved hydrophobicity for organic solvent nanofiltration (OSN) applications [26]. Due to the enhanced performance, $\text{TiO}_2/\text{ZrO}_2$ composite membranes have been commercially available for NF applications [27]. However, open literature on the development of $\text{TiO}_2/\text{ZrO}_2$ composite NF membranes is still scarce.

This study aims to develop $\text{TiO}_2/\text{ZrO}_2$ composite ceramic membranes with different pore sizes for NF. The membrane pore size is determined by the sol size that can be well controlled by adjusting the hydrolysis ratio during sol preparation. The sol properties such as particle size distribution, specific surface area and gas adsorption are systematically investigated. The fabricated composite ceramic membranes are characterized and evaluated in terms of molecular weight cut-off (MWCO), membrane pore size, water flux and salt rejection.

2. Experimental

2.1. Synthesis of composite sols and fabrication of $\text{TiO}_2/\text{ZrO}_2$ membranes

$\text{TiO}_2/\text{ZrO}_2$ composite sols were synthesized through the polymeric sol-gel route. Zirconium n-propoxide (70% in propanol,

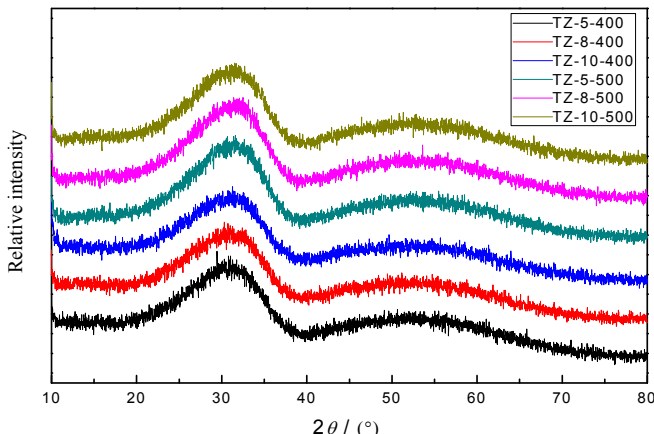


Fig. 2. XRD patterns of the $\text{TiO}_2/\text{ZrO}_2$ powders calcined at 400 and 500 °C.

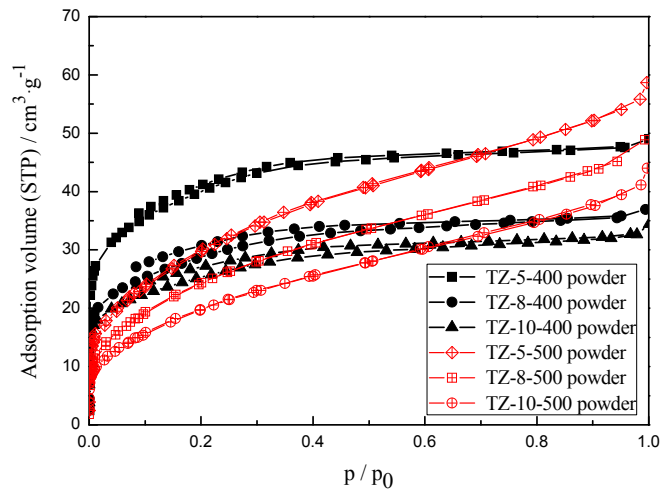


Fig. 3. Nitrogen adsorption–desorption isotherms of the $\text{TiO}_2/\text{ZrO}_2$ powders calcined at 400 and 500 °C.

ABCR GmbH & Co.) and titanium isopropoxide (99% in propanol, ABCR GmbH & Co.) were used as the precursors and diethanolamine (DEA, Shanghai Lingfeng Chemical Reagent Co.) was used as the chelating agent to prevent the complete hydrolysis of the alkoxide in the sol–gel process. The starting alkoxide solution contains $\text{Ti}[\text{OCH}(\text{CH}_3)_2]_4$, $\text{Zr}(\text{OC}_3\text{H}_7)_4$ and DEA with a molar ratio of 1:1:2.4. To obtain sols with different sizes (i.e., 5, 8 and 10 nm), the hydrolysis ratios (i.e. water to alkoxide in molar ratio) were adjusted to 1.3, 2.3 and 3.0. The hydrolysis time and temperature were 90 min and 40 °C, respectively. Detailed procedure for sol preparation can be found in our previous studies [17,28]. For sol characterization, part of the synthesized sols were dried at 45 °C for about 8 h in an oven to get dry powders, and then were calcined at 400 °C and 500 °C with a heating rate of 0.5 °C/min. The resultant $\text{TiO}_2/\text{ZrO}_2$ powders from the sols with different sizes (i.e. 5, 8 and 10 nm) were marked as TZ-5-400, TZ-8-400, TZ-10-400, TZ-5-500, TZ-8-500 and TZ-10-500. The prepared composite membranes were marked in similar ways (e.g., TZ-5 membrane).

$\text{TiO}_2/\text{ZrO}_2$ composite membranes were fabricated via the dip-coating technique, which was performed with an automatic dip-coating device (Velterop DA 3960/02) in a clean room. $\text{TiO}_2/\text{ZrO}_2$ sols were coated onto home-made α -alumina supported mesoporous γ -alumina disks (pore size: 5–6 nm) under clean room (class 1000) conditions. Then the prepared $\text{TiO}_2/\text{ZrO}_2$ composite membrane with one coating layer were calcined at 400 °C for 3 h with a heating and cooling rate of 0.5 °C/min in air.

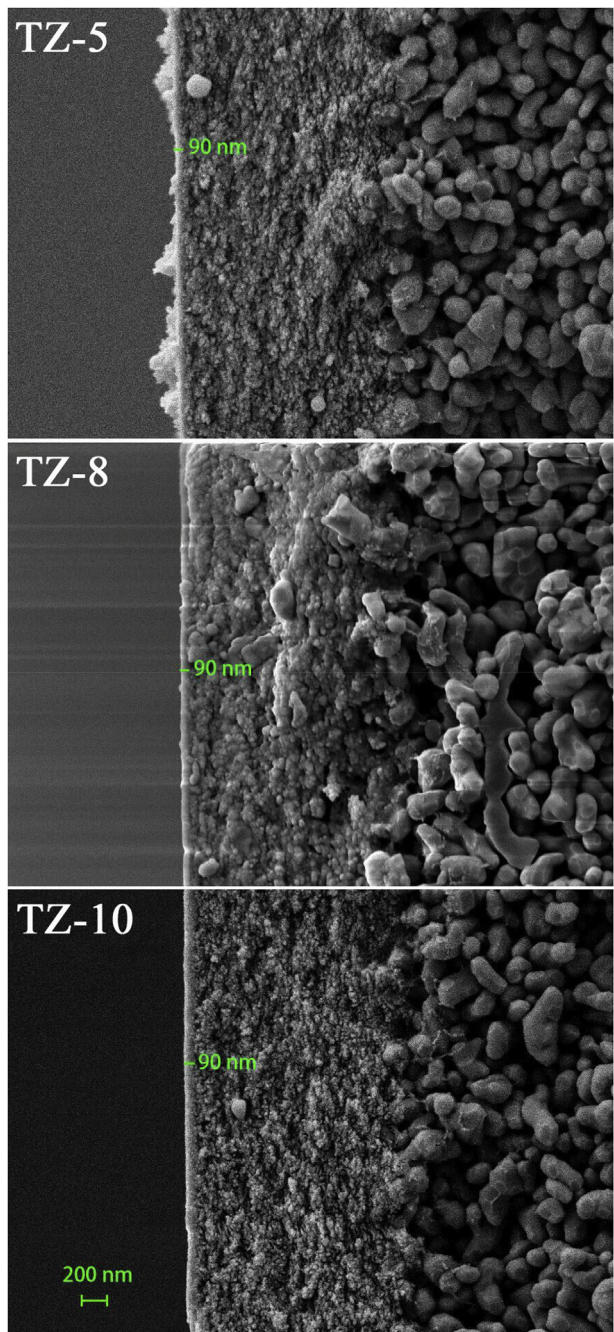
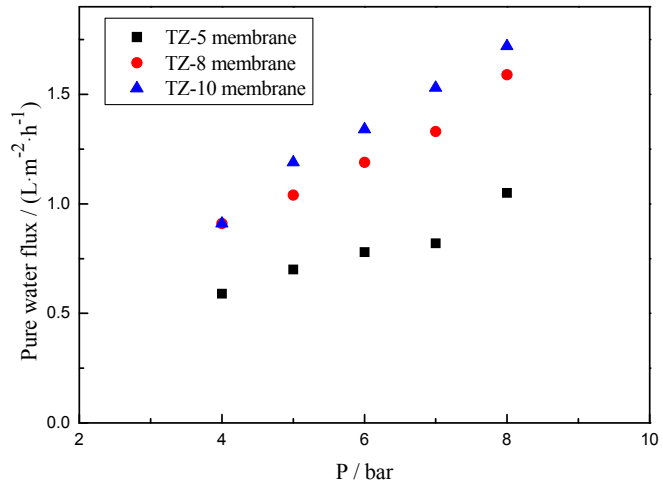
2.2. Sol and powder characterization

Effective particle sizes in the $\text{TiO}_2/\text{ZrO}_2$ composite sols were measured by Dynamic Light Scattering using a Zetasizer analyzer (Nano-ZS90, Malvern). Phase compositions of the composite powders were evaluated by X-ray diffraction (XRD, Bruker D8, Advance diffractometer) with Cu K α radiation operated at 40 kV and 40 mA. The nitrogen adsorption–desorption method was employed to determine the specific surface area and pore structure of the $\text{TiO}_2/\text{ZrO}_2$ powders. The specific surface area of the powder was measured with a surface area and porosity analysis instrument (BELSORP-max, Japan) based on the Brunauer, Emmett and Teller (BET) method.

Zeta potential of the powders in NaCl , MgCl_2 , CaCl_2 and Na_2SO_4 solutions were measured with a zeta potential analyzer (Zetasizer Nano ZS90, Malvern). 0.02 g $\text{TiO}_2/\text{ZrO}_2$ powders were dissolved into

Table 1Properties of $\text{TiO}_2/\text{ZrO}_2$ composite powders calcined at different temperatures.

Powders	N_2 adsorption–desorption isotherms	V_{micro} $/\text{cm}^3 \cdot \text{g}^{-1}$	V_{total} $/\text{cm}^3 \cdot \text{g}^{-1}$	$V_{\text{micro}}/V_{\text{total}}$ %	BET surface area/ $\text{m}^2 \cdot \text{g}^{-1}$
TZ-5-400	Type I	0.0552	0.0734	75.20	144.5
TZ-8-400	Type I	0.0394	0.0556	70.86	102.9
TZ-10-400	Type I	0.0349	0.0500	69.80	90.75
TZ-5-500	Type II	0.0373	0.0857	43.52	112.7
TZ-8-500	Type II	0.0300	0.0715	41.96	92.61
TZ-10-500	Type II	0.0245	0.0614	39.90	74.44

**Fig. 4.** SEM images of the membrane cross-sections.100 mL salt solution (0.005 mol/L). 0.1 mol/L HCl or $\text{NH}_3 \cdot \text{H}_2\text{O}$ **Fig. 5.** Water flux of the three $\text{TiO}_2/\text{ZrO}_2$ membranes as a function of transmembrane pressure.

solution was used to adjust pH of the solution to various values. Zeta potential measurements were performed after 5-min stabilization.

2.3. Membrane characterization

The cross-sections of the $\text{TiO}_2/\text{ZrO}_2$ composite membranes were characterized with field-emission scanning electron microscope (FESEM, Hitachi S4800), operating at an accelerating voltage of 3 kV. Pure water fluxes of the membranes were evaluated with a dead-end filtration apparatus [17] under transmembrane pressures up to 0.8 MPa. Molecular weight cut-off (MWCO) properties of the composite membranes were investigated with the same filtration apparatus. Polyethylene glycol (PEG) with different molecular weights, i.e., 200, 600 and 1500 (Alfa Aesar) was used to prepare a 3 g/L feed solution. The PEG retention experiment was performed under a feed solution stirring rate of 200 r/min and a transmembrane pressure of 0.76 MPa at a temperature of 25 ± 2 °C. The membrane retention was determined by the measurement of the feed and permeate concentrations with gel permeation chromatography (GPC, Waters). The molecular weight of PEG corresponding to a 90% retention level was taken as the MWCO of the composite membranes.

Salt retentions of the membranes to single-component salts including MgCl_2 , CaCl_2 , Na_2SO_4 and NaCl were determined with the same filtration apparatus under transmembrane pressures up to 0.8 MPa at ambient temperature (25 ± 2 °C). In each filtration, the feed solution was stirred at a speed of 200 r/min and pressurized for 1 h. The feed concentration and pH were controlled in the range of 0.005–0.1 mol/L and 6.0 (by adding HNO_3 or $\text{NH}_3 \cdot \text{H}_2\text{O}$), respectively. After 1-h permeation, the feed and permeate

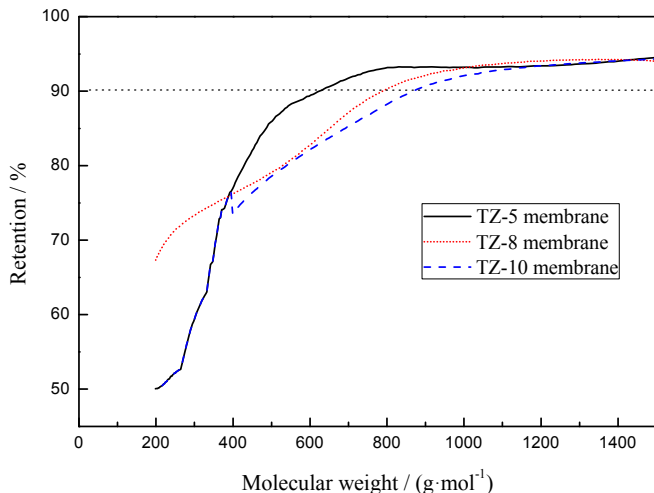


Fig. 6. PEG retention of the three $\text{TiO}_2/\text{ZrO}_2$ membranes calcined at $400\text{ }^\circ\text{C}$.

concentrations were determined with a conductivity meter (DDS-307, Shanghai Leici Instrument Factory). Salt rejection (i.e., retention) R of the membrane can be expressed by the following equation:

$$R(\%) = \left(1 - \frac{C_p}{C_f}\right) \times 100 \quad (1)$$

where C_p and C_f are the concentrations of permeate and feed solutions, respectively.

3. Results and discussion

3.1. Particle size distributions of the sols

In this study, three freshly prepared $\text{TiO}_2/\text{ZrO}_2$ composite sols derived from different hydrolysis ratios (1.3, 2.3 and 3.0) are clear and transparent. Their particle size distributions are displayed in Fig. 1. All the sols exhibit uni-modal distributions, with mode particle sizes of 4.9, 7.9 and 10.1 nm. In Fig. 1, it is obvious that the particle size distribution becomes wider and the sol size becomes larger with the rise in hydrolysis ratio. Wider particle size distribution and larger sol size indicate the occurrence of faster hydrolysis and polycondensation reactions and the formation of highly branched cluster in the sol. In membrane fabrication, the sol size generally should be no less than the pore size of the intermediate layer (5–6 nm in this study) to prevent sol penetration into the intermediate layer. However, the sol size should also be small enough so that the prepared membrane has reasonable salt rejections.

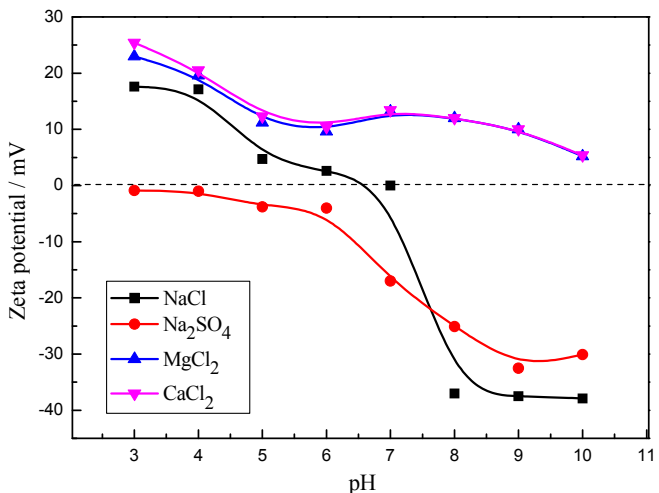


Fig. 7. Zeta potential of the $\text{TiO}_2/\text{ZrO}_2$ composite membrane in different salt solutions under various pH values.

3.2. Properties of the composite powders (i.e., unsupported membranes)

Powders calcined at different temperatures are generally regarded as unsupported membranes, and their properties reflect the properties of the membranes at the corresponding calcination temperatures. XRD patterns of the $\text{TiO}_2/\text{ZrO}_2$ composite powders are shown in Fig. 2. It can be seen that all composite powders exhibit similar XRD patterns, namely, similar phase compositions and amorphous structures at the calcination temperatures of 400 and $500\text{ }^\circ\text{C}$. For pure ZrO_2 powders, phase transition temperature of the amorphous structure is $\sim 350\text{ }^\circ\text{C}$ [28]; for pure TiO_2 powders, phase transition temperature of the amorphous structure is $\sim 400\text{ }^\circ\text{C}$ [22]. In the present study, the structure of the powder is still in amorphous phase when the calcinations temperature is up to $500\text{ }^\circ\text{C}$. Obviously, the crystallization temperature of the mixed $\text{TiO}_2/\text{ZrO}_2$ powder has been significantly increased compared with the pure oxide powder. The transition temperature from amorphous to crystalline phase of $\text{TiO}_2/\text{ZrO}_2$ was reported at $\sim 650\text{ }^\circ\text{C}$ [29,30] or even higher [31], depending on sol preparation conditions.

Fig. 3 shows nitrogen adsorption–desorption isotherms (at 77 K) of the $\text{TiO}_2/\text{ZrO}_2$ powders calcined at 400 and $500\text{ }^\circ\text{C}$. The powders calcined at $400\text{ }^\circ\text{C}$ exhibit type I isotherms that correspond to microporous structures, while the powders calcined at $500\text{ }^\circ\text{C}$ exhibit type II isotherms, suggesting non-microporous structures. Obviously, $400\text{ }^\circ\text{C}$ is preferable as the calcination temperature in membrane fabrication. As expected, the gas absorption capacity decreases with the increase of the sol size. These results are in agreement with the data in Table 1.

The micropore volume and the total volume are corresponding to the adsorption volumes at relative pressures of 0.1 and 0.95, respectively. From Table 1, we can see that the volume of the micropores and the ratio of micropore volume to the total volume

Table 2

Estimated membrane properties based on the measured water flux (assuming pore size and porosity of the support layer are 5 nm and 35%, respectively).

Sample	Water permeability ($\times 10^{-12} \text{ m s}^{-1} \text{ Pa}^{-1}$)	Resistance ($\times 10^{14} \text{ m}^{-1}$)	R_{support}/R_m	Pore size (nm)	Porosity (%)
Support	5.56	2.01	—	5	35
$M_{\text{TZ-5}}$	0.33	33.91	0.059	1.2	1.9
$M_{\text{TZ-8}}$	0.53	21.11	0.095	1.4	2.3
$M_{\text{TZ-10}}$	0.61	18.61	0.108	1.5	2.4

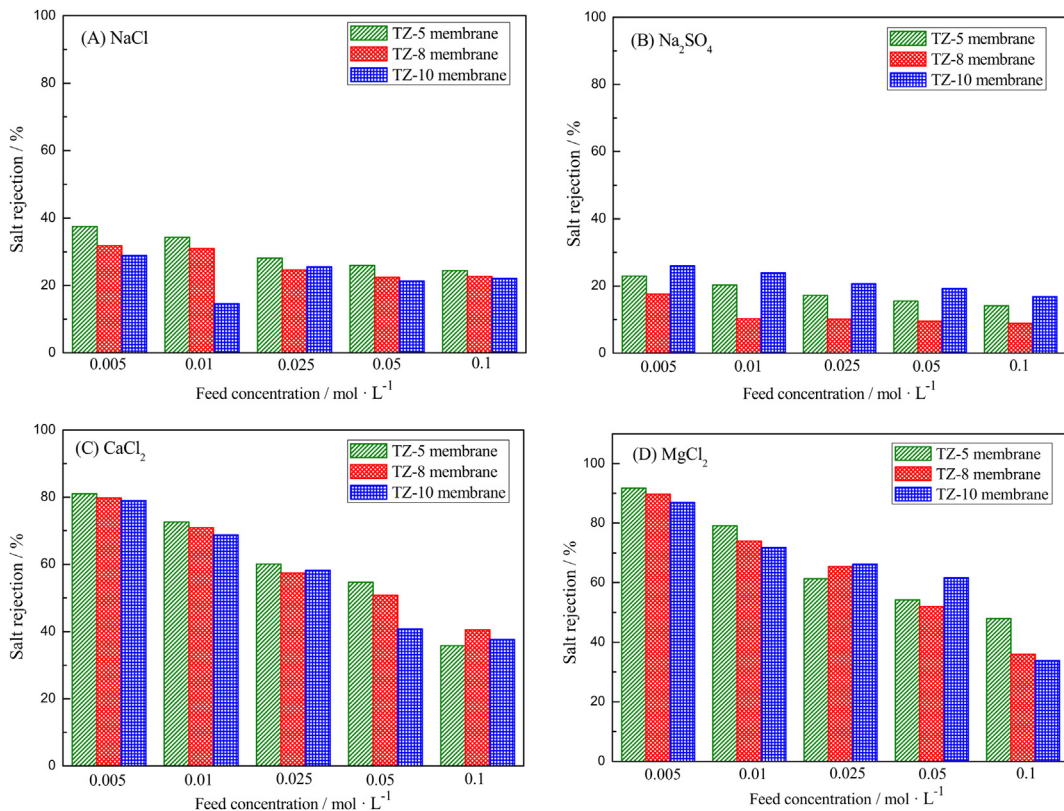


Fig. 8. Rejection performance of the $\text{TiO}_2/\text{ZrO}_2$ composite membranes to different salts as a function of the feed concentration: (A) NaCl , (B) Na_2SO_4 , (C) CaCl_2 and (D) MgCl_2 . Test conditions: temperature $25 \pm 2^\circ\text{C}$, feed solution pH = 6, transmembrane pressure 8 bar, and stirring rate 200 r/min.

decrease significantly from TZ-5-400 to TZ-10-500. The BET data also confirms that the powders calcined at 500°C have much lower specific surface area compared with the powders calcined at 400°C . The specific surface area of TZ-10-500 is only half of that of TZ-5-400. Due to the lower specific surface area of the powder calcined at 500°C , 400°C was selected as the calcination temperature in membrane preparation.

3.3. Membrane morphology

Fig. 4 displays the cross-sections of the three membranes. The relatively porous α -alumina substrate, the mesoporous γ -alumina intermediate layer and top selective layer are clear visible. It is also obvious that the three membranes have very similar and thin top selective layers. The thickness of the top selective layer is around 90 nm, which is much thinner than BTESE membranes (e.g., 440–550 nm [32]) and Zr-BTESE membranes (e.g., 150–300 nm [33]). The thin top layer is supposed to benefit the mass transfer across the membrane.

3.4. Nanofiltration performance

Fig. 5 describes water flux performance of the three $\text{TiO}_2/\text{ZrO}_2$ composite membranes. The ceramic membrane derived from the sol with larger size (e.g., the TZ-10 membrane) exhibits higher water flux than the membrane derived from the sol with smaller size. The TZ-5 membrane shows relatively low water permeability ($0.33 \times 10^{-12} \text{ m s}^{-1} \text{ Pa}^{-1}$). This is supposed to be caused by the small sol size. The corresponding sol size is only 5 nm, while the pore size of the intermediate layer is 5–6 nm. As a result, the sol may block the pore of the intermediate layer, leading to the low water flux of the TZ-5 membrane. Water fluxes of the TZ-8 and TZ-

10 membranes are also relatively low, suggesting small membrane pore size and/or low porosity. The assumption is confirmed by the following results.

PEG rejections of the $\text{TiO}_2/\text{ZrO}_2$ membranes are illustrated in **Fig. 6**. The molecular weight is regarded as MWCO of the membrane when the PEG rejection is 90%. From **Fig. 6**, we can determine that the three composite membranes have MWCOs of 620, 788 and 860 Da. This indicates that the membrane pore size increases from TZ-5 to TZ-8 to TZ-10, which is in agreement with the water flux behaviours. In the future study, the membrane microstructure (e.g., pore size and microporosity) is required to be further optimized so that high water permeability and high salt rejection can be achieved.

Based on the relation between the molecular weight of PEG and pore size, the average pore size of the composite membrane can be evaluated via the following equation [10].

$$r = 0.262 \times (M_W)^{0.5} - 0.3 \quad (2)$$

Where r is the pore radius of membrane (\AA) and M_W is the molecular weight of PEG (g mol^{-1}).

The calculated pore sizes of the TZ-5, TZ-8 and TZ-10 membranes are 1.2, 1.4 and 1.5 nm, respectively. Ceramic membranes with pore sizes in the range of 1–2 nm and MWCO in the range of 200–1000 Da are generally regarded to be suitable for NF applications [23]. Therefore, the prepared composite ceramic membranes can be employed for NF.

In pressure driven membrane processes, mass transfer resistance of the selective layer and support layer can be expressed by the resistance-in-series model, similar to the layered resistance in membrane fouling [34]:

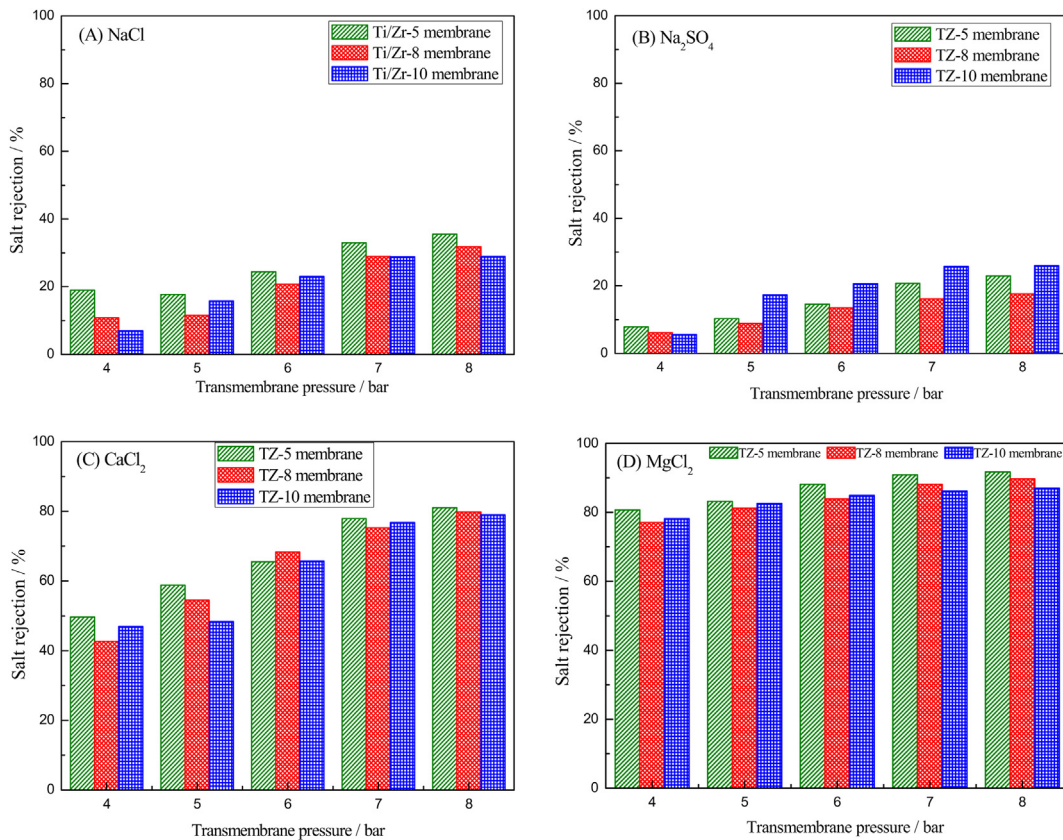


Fig. 9. Rejection performance of the $\text{TiO}_2/\text{ZrO}_2$ composite membranes to different salts as a function of the transmembrane pressure: (A) NaCl , (B) Na_2SO_4 , (C) CaCl_2 and (D) MgCl_2 . Test conditions: temperature $25 \pm 2^\circ\text{C}$, feed solution pH = 6, feed concentration 0.005 mol/L, and stirring rate 200 r/min.

Table 3
Crystal and hydrated radii of Na^+ , Ca^{2+} , Mg^{2+} , Cl^- and SO_4^{2-} .

Ions	Crystal radii (nm) [36]	Hydrated radii (nm) [37]
Na^+	0.102	0.358
Ca^{2+}	0.123	0.412
Mg^{2+}	0.072	0.428
Cl^-	0.181	0.332
SO_4^{2-}	0.215	0.300

$$J = \frac{\Delta P}{\mu R_m} = \frac{\Delta P}{\mu(R_{\text{selective}} + R_{\text{support}})} \quad (3)$$

where J is the water flux (m s^{-1}), ΔP is the transmembrane pressure (Pa), μ is the water viscosity (Pa s), and R_m , $R_{\text{selective}}$ and R_{support} are the resistance (m^{-1}) from the whole membrane, the selective layer and the support (intermediate layer + substrate), respectively.

According to the Hagen–Poiseuille equation [35], the water flux can be described by

$$J = \frac{\Delta P d^2 \varepsilon}{32 \mu L \tau} \quad (4)$$

where d is the pore diameter (m), ε is porosity (dimensionless), τ is tortuosity (dimensionless) and L is thickness (m).

Based on equations (3)–(4) and the measured water flux, the membrane water permeability, resistance, pore size and porosity are summarized in Table 2. It can be seen that resistance of the support layer (including the substrate) accounts for a small portion (6–11%) of the total membrane resistance. Namely, mass transfer resistance of the membrane is mainly caused by the dense selective

layer. The calculated porosity of the selective layer is very low (1.9–2.4%), resulting in low water flux. In the future, the porosity should be optimised to achieve high water flux and salt rejection.

NF membranes are generally negatively or positively charged. Their salt rejection behaviours are closely related to the surface charge of the membrane due to separation mechanisms of the Donnan effect and double electrical layer exclusion [7,17]. Fig. 7 illustrates zeta potential of the composite membrane in different salt solutions under various pH values. It is found that the membrane is positively charged in CaCl_2 and MgCl_2 solutions, and negatively charged in Na_2SO_4 solution within the pH range of 3–10. For NaCl solution, the membrane shows amphoteric properties; namely, it is positively charged when $\text{pH} < 7$ and negatively charged when $\text{pH} > 7$.

Fig. 8 and Fig. 9 show salt rejections of the $\text{TiO}_2/\text{ZrO}_2$ composite membranes to NaCl , Na_2SO_4 , CaCl_2 and MgCl_2 under different feed concentrations and transmembrane pressures, respectively. It can be seen that the membranes exhibit lower rejections to NaCl and Na_2SO_4 , but higher rejections to CaCl_2 and MgCl_2 . Rejections of the membranes to four types of salts at the pH of 6 are in the order: $\text{Na}_2\text{SO}_4 < \text{NaCl} < \text{CaCl}_2 < \text{MgCl}_2$, which is the same to the order of the ZrO_2 membranes developed in our group [17]. The salt rejection performance can be explained by the Donnan exclusion mechanism. At pH = 6, the $\text{TiO}_2/\text{ZrO}_2$ membranes are positively charged in NaCl , CaCl_2 and MgCl_2 solutions and the charge density is in the order: $\text{NaCl} < \text{CaCl}_2 < \text{MgCl}_2$ (Fig. 7). As a result, the membrane exhibits higher retentions for cations (e.g., Ca^{2+} and Mg^{2+}) due to the Donnan exclusion effect.

The salt rejection order of the membranes also agrees well with the hydrated radii of the ions: $\text{SO}_4^{2-} < \text{Cl}^- < \text{Na}^+ < \text{Ca}^{2+} < \text{Mg}^{2+}$ (Table 3) [36,37]. It is reported that the hydrated radii of ions play

an important role in ion transport and thus retention in NF [38]. Therefore, the hydration related size effect may also have an influence on the transfer mechanism of the fabricated $\text{TiO}_2/\text{ZrO}_2$ ceramic NF membranes in the single-component solution system.

Figs. 8 and 9 also describe that salt rejection of the membrane decreases with the increase in feed concentration and increases with the rise in transmembrane pressure. These results have been confirmed in numerous NF studies [7,10,17,23–25,38,39]. Diffusion (due to concentration gradient), convection (due to pressure gradient) and electromigration (due to electrical potential gradient) have been employed to explain the results [7,10,17,39].

4. Conclusions

We have successfully fabricated $\text{TiO}_2/\text{ZrO}_2$ ceramic NF membranes via the polymeric sol–gel and dip-coating techniques. The unsupported and supported composite ceramic membranes are systematically characterized and evaluated in terms of phase composition, chemical stability, gas adsorption, molecular weight cut-off (MWCO), membrane pore size, water flux and salt rejection. The prepared $\text{TiO}_2/\text{ZrO}_2$ ceramic membranes have amorphous phase at 400 and 500 °C, suggesting the high thermal stability. The fabricated membranes have the MWCO of 620–860 Da, corresponding to the membrane pore size of 1.2–1.5 nm. Relatively low water permeability can be attributed to the low microporosity of the membrane. Further optimization of the membrane microstructure is required to improve the membrane permeability in the future. It is proved that Donnan exclusion is the dominant transport mechanism of the NF membrane in the single-component system, and that salt rejection is also related to the hydration properties of the ions (e.g., the hydration radius).

Acknowledgements

This work is supported by the National Natural Science Foundation of China (21276123, 21490581), the National High Technology Research and Development Program of China (2012AA03A606) and the “Summit of the Six Top Talents” Program of Jiangsu Province. We also would like to thank Mrs Huating Song and Maowen Yue for their great help with the figure drawing and insightful discussion.

References

- [1] R. Weber, H. Chmiel, V. Mavrov, Desalination 157 (2003) 113–125.
- [2] S. Condom, A. Larbot, S. Alami Younssi, M. Persin, Desalination 168 (2004) 207–213.
- [3] F.C. Kramer, R. Shang, S.G.J. Heijman, S.M. Scherrenberg, J.B. van Lier, L.C. Rietveld, Sep. Purif. Technol. 147 (2015) 329–336.
- [4] A.W. Mohammad, Y.H. Teow, W.L. Ang, Y.T. Chung, D.L. Oatley-Radcliffe, N. Hilal, Desalination 356 (2015) 226–254.
- [5] S. Benfer, U. Popp, H. Richter, C. Siewert, G. Tomandl, Sep. Purif. Technol. 22–23 (2001) 231–237.
- [6] T. Van Gestel, C. Vandecasteele, A. Buekenhoudt, C. Dotremont, J. Luyten, B. Van der Bruggen, G. Maes, J. Membr. Sci. 214 (2003) 21–29.
- [7] J. Schaepl, C. Vandecasteele, B. Peeters, J. Luyten, C. Dotremont, D. Roels, J. Membr. Sci. 163 (1999) 229–237.
- [8] T. Kuzniatsova, M.L. Mottern, K. Shqau, D. Yu, H. Verweij, J. Membr. Sci. 316 (2008) 80–88.
- [9] H. Grib, M. Persin, C. Gavach, D.L. Piron, J. Sandeaux, N. Mameri, J. Membr. Sci. 172 (2000) 9–17.
- [10] P. Puhlfürß, A. Voigt, R. Weber, M. Morbé, J. Membr. Sci. 174 (2000) 123–133.
- [11] T. Van Gestel, C. Vandecasteele, A. Buekenhoudt, C. Dotremont, J. Luyten, R. Leysen, B. Van der Bruggen, G. Maes, J. Membr. Sci. 209 (2002) 379–389.
- [12] J. Sekulić, J.E. ten Elshof, D.H.A. Blank, Adv. Mater. 16 (2004) 1546–1550.
- [13] T. Tsuru, D. Hironaka, T. Yoshioka, M. Asaeda, Desalination 147 (2002) 213–216.
- [14] T. Van Gestel, C. Vandecasteele, A. Buekenhoudt, C. Dotremont, J. Luyten, R. Leysen, B. Van der Bruggen, G. Maes, J. Membr. Sci. 207 (2002) 73–89.
- [15] T. Van Gestel, H. Kruidhof, D.H.A. Blank, H.J.M. Bouwmeester, J. Membr. Sci. 284 (2006) 128–136.
- [16] T. Van Gestel, D. Sebold, H. Kruidhof, H.J.M. Bouwmeester, J. Membr. Sci. 318 (2008) 413–421.
- [17] H. Qi, G. Zhu, L. Li, N. Xu, J. Sol-Gel Sci. Technol. 62 (2012) 208–216.
- [18] P. Blanc, A. Larbot, J. Palmeri, M. Lopez, L. Cot, J. Membr. Sci. 149 (1998) 151–161.
- [19] J. Palmeri, P. Blanc, A. Larbot, P. David, J. Membr. Sci. 179 (2000) 243–266.
- [20] C.H. Chang, R. Gopalan, Y.S. Lin, J. Membr. Sci. 91 (1994) 27–45.
- [21] X. Chen, W. Zhang, Y. Lin, Y. Cai, M. Qiu, Y. Fan, Microporous Mesoporous Mater. 214 (2015) 195–203.
- [22] U. Aust, S. Benfer, M. Dietze, A. Rost, G. Tomandl, J. Membr. Sci. 281 (2006) 463–471.
- [23] T. Tsuru, S.-i. Wada, S. Izumi, M. Asaeda, J. Membr. Sci. 149 (1998) 127–135.
- [24] T. Tsuru, T. Sudoh, T. Yoshioka, M. Asaeda, J. Membr. Sci. 185 (2001) 253–261.
- [25] Y. Cai, X. Chen, Y. Wang, M. Qiu, Y. Fan, Microporous Mesoporous Mater. 201 (2015) 202–209.
- [26] S. Zeidler, P. Puhlfürß, U. Kätzel, I. Voigt, J. Membr. Sci. 470 (2014) 421–430.
- [27] C. Mazzoni, F. Orlandini, S. Bandini, Desalination 240 (2009) 227–235.
- [28] G. Zhu, Q. Jiang, H. Qi, N. Xu, Chin. J. Chem. Eng. 23 (2015) 31–41.
- [29] M.C. Hu, E.A. Payzant, K.R. Booth, C.J. Rawn, R.D. Hunt, L.F. Allard, J. Mater. Sci. 38 (2003) 3831–3844.
- [30] S. Naci Koç, J. Sol-Gel Sci. Technol. 38 (2006) 277–281.
- [31] S. Ananta, R. Tipakontitkul, T. Tunkasiri, Mater. Lett. 57 (2003) 2637–2642.
- [32] H.L. Castricum, H.F. Qureshi, A. Nijmeijer, L. Winnubst, J. Membr. Sci. 488 (2015) 121–128.
- [33] M. ten Hove, A. Nijmeijer, L. Winnubst, Sep. Purif. Technol. 147 (2015) 372–378.
- [34] R. Fabris, E.K. Lee, C.W.K. Chow, V. Chen, M. Drikas, J. Membr. Sci. 289 (2007) 231–240.
- [35] M. Hayama, F. Kohori, K. Sakai, J. Membr. Sci. 197 (2002) 243–249.
- [36] M.Y. Kiriukhin, K.D. Collins, Biophys. Chem. 99 (2002) 155–168.
- [37] A.G. Volkov, S. Paula, D.W. Deamer, Bioelectrochem. Bioenerg. 42 (1997) 153–160.
- [38] B. Tansel, J. Sager, T. Rector, J. Garland, R.F. Strayer, L. Levine, M. Roberts, M. Hummerick, J. Bauer, Sep. Purif. Technol. 51 (2006) 40–47.
- [39] T. Tsuru, D. Hironaka, T. Yoshioka, M. Asaeda, Sep. Purif. Technol. 25 (2001) 307–314.